

IMPULSIVE AND GRADUAL NONTHERMAL EMISSIONS IN AN X-CLASS FLARE

JIONG QIU, JEONGWOO LEE, AND DALE E. GARY

Center For Solar Research, Physics Department, New Jersey Institute of Technology, 323 Martin Luther King Boulevard, Newark, NJ 07102-1982

Received 2002 October 29; accepted 2003 November 13

ABSTRACT

In this paper we present a comprehensive case study of an X-class flare observed on 2001 April 6. The flare consists of two episodes, the first characterized by impulsive spiky bursts and the second by gradual smooth emission at hard X-ray and microwave wavelengths. Emissions in the two episodes are regarded as the impulsive and gradual components, respectively. We compare the temporal, spatial, and spectral evolution of the two components in hard X-rays and microwaves. For this event, the most important finding is that both the impulsive and gradual hard X-rays at ≥ 50 keV are thick-target emissions at conjugate footpoints. Evolution of hard X-rays and microwaves during the gradual phase exhibits a separation motion between two footpoint sources, which reflects progressive magnetic reconnection. Observations further reveal distinct spectral properties of the gradual component. It is most prominently observed in the high-energy (>20 keV) range, and the gradual hard X-rays have a harder and hardening spectrum compared with the impulsive component. The gradual component is also a microwave-rich event, with the microwaves lagging the hard X-rays by tens of seconds. A correlation analysis of the hard X-ray light curves shows energy-dependent time delays, with the 200 keV hard X-rays lagging the 40 keV emission by 20 s. The observations and analyses suggest that magnetic reconnection occurs during both the impulsive and gradual phases that generate nonthermal electrons, primarily precipitating at the footpoints. However, the temporal and spectral properties of the gradual component must be produced by an acceleration mechanism different from that of the impulsive phase. We propose that the “collapsing-trap” effect, as a product of progressive magnetic reconnection in bipolar magnetic fields, is a viable mechanism that continuously accelerates the gradual-phase electrons in a low-density trap before they precipitate into the footpoints.

Subject headings: Sun: activity — Sun: flares — Sun: radio radiation — Sun: X-rays, gamma rays

1. INTRODUCTION

Studies of emissions at hard X-ray and microwave wavelengths provide key information on mechanisms of acceleration and transport of flare-produced electrons. On the basis of hard X-ray and microwave time profiles, it has been recognized that flare-associated high-energy bursts can be categorized into two general types, namely, impulsive and gradual emissions. The impulsive emissions have a short timescale, of order several tens of seconds to a few minutes, and the gradual emissions evolve over a longer timescale of tens of minutes. The distinction between the two turns out to be more than superficial and is not limited to temporal properties. Statistical and case studies in the last two decades (Kosugi, Dennis, & Kai 1988 and references therein), and most recently by Silva, Wang, & Gary (2000), revealed other respects in which the impulsive and gradual emissions show contrasting properties. These include (1) the microwaves in the gradual events show greater time delays, by more than a few tens of seconds, with respect to the hard X-rays than in the impulsive events (Silva et al. 2000); (2) the gradual events exhibit a harder and hardening (soft-hard-harder, or SHH) spectrum compared with the impulsive events, which exhibit a soft-hard-soft (SHS) spectrum (Silva et al. 2000); and (3) the gradual bursts are usually microwave-rich events, and statistically the ratio of the microwave to hard X-ray flux is larger in the gradual events than in the impulsive events by a factor of 5 (Kosugi et al. 1988; Silva et al. 2000). The most critical issue is whether these contrasting properties between impulsive and gradual emissions are produced by different acceleration mechanisms or merely represent transport effects, such as precipitation

versus trapping, due to different properties of the ambient plasmas and magnetic configurations.

Regardless of the impulsive or gradual nature of the bursts, both trapping and acceleration models have been developed to explain the energy-dependent time profiles. In terms of trapping, on the basis of the great similarity of the hard X-ray and microwave time profiles, Takakura & Kai (1966) first proposed the scenario that nonthermal electrons are fully trapped in the corona and emit hard X-rays through thin-target bremsstrahlung and microwaves through gyrosynchrotron radiation. It has often been reported that hard X-rays at higher energies are delayed with respect to lower energy emissions. Takakura & Kai (1966), Bai & Ramaty (1979), and Vilmer, Kane, & Trotter (1982) put forward the trapping scenario and considered such energy-dependent time delays to be caused by the energy-loss rate of electrons in the trap. On the other hand, some observed temporal and spectral properties that are interpreted as due to trapping effects can also be explained by acceleration mechanisms. Bai & Ramaty (1979) proposed a two-step acceleration to explain the time delay of higher energy hard X-rays with respect to lower energy emissions. Miller, LaRosa, & Moore (1996) developed stochastic acceleration models in which a second-order acceleration can switch on with the already accelerated seed electrons. Furthermore, Melrose & Brown (1976) suggested that both the impulsive and gradual X-rays can be emitted by precipitating electrons, which, however, have different pitch-angle distributions. Bifurcations in the initial pitch-angle distributions imply different acceleration mechanisms. Given that acceleration theories could produce a nonnegligible time delay comparable to the observed timescales, Lu & Petrosian (1990)

proposed that a continuous acceleration may explain the spectral hardening if more high-energy electrons are generated as the flare evolves. Furthermore, Melrose & Brown (1976) and MacKinnon (1988, 1991) implemented trap-plus-precipitation models, which were tested by Aschwanden et al. (1997) by applying correlation analysis to hard X-ray observations. Recently, Somov & Kosugi (1997) put forward the concept of a “collapsing” magnetic trap, which they consider to provide a second-step acceleration mechanism. They argued that efficiency of the second-step acceleration depends on the plasma properties (such as density) at the energy release site and inside the trap.

To test the models, it is most desired to analyze coordinated, spectrally and spatially resolved observations at X-rays and microwaves. To explain the observed distinction between impulsive and gradual events, Kosugi et al. (1988) adopted the coronal trapping scenario in interpreting the energy-dependent temporal correlation between hard X-rays and microwaves in the gradual bursts, while the impulsive bursts were considered to be thick-target sources of strong magnetic fields due to precipitating nonthermal electrons. On the other hand, an interesting event was presented by MacKinnon et al. (1986), in which the hard X-ray and microwave bursts underwent two stages in which the emissions in many respects resemble the impulsive and gradual bursts, respectively. MacKinnon et al. (1986) proposed a scenario different from that of Kosugi et al. (1988) and suggested that in both stages the hard X-rays are thick-target emissions by low-energy (~ 100 keV) electrons, while microwaves are emitted by high-energy (up to MeV) electrons. They attributed the difference between the impulsive and gradual components to the fact that electrons for the gradual bursts have an energy spectrum different from that for the impulsive bursts, which they believed to be produced by different acceleration mechanisms during the evolution of the flare.

The competing scenarios for the gradual bursts can be most efficiently distinguished by imaging spectroscopy of nonthermal emissions (e.g., Metcalf & Alexander 1999). Many imaging observations from the *Yohkoh* Hard X-Ray Telescope (HXT; Kosugi et al. 1991) revealed the thick-target nature of hard X-rays above 30 keV for most flares (Sakao 1994). Using observations by *Hinotori*, Tsuneta et al. (1984) and Nitta, Kiplinger, & Kai (1989) found some events with gradual X-ray components at less than 50 keV that are loop-top sources. They argued that the observed gradual components are emitted by nonthermal electrons trapped at the loop top, which were difficult to isolate from the superhot (≥ 30 MK) sources. In a limb event, Masuda et al. (1994) discovered a loop-top, nonthermal, hard X-ray source that evolves with thick-target footpoint sources. These observations so far have not been enough to provide a convincing explanation of the spectral properties of the gradual nonthermal bursts summarized by Kosugi et al. (1988) and Silva et al. (2000). To understand the nature of gradual nonthermal bursts, it is important to combine the spatially resolved observations and spectral evolution of the nonthermal bursts in more events. Furthermore, in disk events, it can become difficult to distinguish loop-top and footpoint sources because of projection effects. Coordinated observations at multiple wavelengths provide important information on the magnetic configuration of the flare, which will help remove such ambiguity in some disk events.

In this paper, we present a comprehensive case study of an X5.6 flare event observed by several instruments on 2001 April 6 (§ 2), which consists of multiple impulsive peaks and a

gradual component arising 20 minutes after the impulsive onset (§ 3). From the imaging observations, it is straightforward to tell whether the hard X-rays are primarily thick- or thin-target sources and what are the magnetic fields in the source regions of the nonthermal emissions (§ 3). From the spectral analysis, we study the evolution of nonthermal electrons from the impulsive to the gradual bursts (§ 4). In § 5, we also derive time lags between hard X-rays at different energies and between hard X-rays and microwaves. In § 6, we discuss the collapsing-trap mechanism, which we suggest as a possible acceleration mechanism to explain the observed gradual phase properties, and conclusions are given in § 7.

2. INSTRUMENTS AND DATA

The X5.6 flare on 2001 April 6 occurred in the NOAA Active Region 9415 (S21° E31°). It was one of the largest flares during solar cycle 23 and was observed by various ground-based and satellite-borne instruments. This event is associated with a fast halo coronal mass ejection (CME), the speed of its front being 1200 km s^{-1} . For our purpose of investigating the properties of flare-generated electrons, we put emphasis on studies of multichannel hard X-ray observations by the HXT (Kosugi et al. 1991) and Wide Band Spectrometer (WBS; Yoshimori et al. 1991) on board *Yohkoh* and multifrequency microwave observations obtained by Owens Valley Solar Array (OVSA; Gary & Hurford 1990).

The *Yohkoh* HXT observed the flare at four energy channels, L, M1, M2, and H (14–23–33–53–93 keV), with a cadence of 0.5 s. The standard analysis software for reconstructing hard X-ray images uses the maximum entropy method (Sakao 1994), with an improved calibration pattern (Sato, Kosugi, & Makishima 1999). The image resolution (FWHM) is typically $5''$ – $10''$. The four-channel measurements are well calibrated, allowing us to build the hard X-ray photon spectrum. We also use data from the Hard X-Ray Spectrometer (HXS), which is part of the WBS. Its pulse-height detector records photons from 25 to 850 keV, distributed in 32 energy channels, and the time cadence is 1 s. In this event, significant emission was observed by WBS at up to 400 keV, and observations from the WBS HXS are presented in this paper.

OVSA is a solar-dedicated, frequency-agile interferometer, which currently consists of two 27 m antennas and four 2 m antennas. Its receiver can be tuned to harmonics of 200 MHz in the range of 1.0–18.0 GHz. It provides measurements of the amplitude, phase, total power, and circularly polarized radiation. The temporal resolution of the measurements depends on the number of frequencies used during the observation. For the event studied in this paper, OVSA was observing at 40 frequencies, yielding a time cadence of 4 s for the total power and 8 s for the polarization measurements. The combination of six antennas gives 15 baseline measurements, from which microwave images at various frequencies can be obtained using the standard CLEAN method Högbom (1974). The four 2 m antennas view the whole solar disk, and the two 27 m antennas only look at a part of the Sun, the field of view being inversely proportional to the working frequency.

We also exploit observations at other wavelengths, such as soft X-ray light curves from *GOES*, soft X-ray images from the *Yohkoh* Soft X-Ray Telescope (SXT; Tsuneta et al. 1991), and longitudinal magnetograms from the Michelson Doppler Imager (MDI; Scherrer et al. 1995) on the *Solar and Heliospheric Observatory* (*SOHO*; Domingo, Fleck, & Poland 1995), to retrieve information on the spatial and magnetic

properties of the flare. We register images observed at different wavelengths according to the pointing coordinates of various instruments, and offsets between images at different times due to solar rotation are taken into account. The co-alignment accuracy is of the order of a few arcseconds.

3. EVOLUTION OF THE FLARE

In this section, we study the evolution of the flare at X-ray and radio wavelengths. We present the light curves of the X-ray count rates in multiple energy channels and the microwave total power flux at various frequencies, which demonstrate that the evolution of the emission consists of both impulsive and gradual components. We also derive images at both wavelengths to locate the sources of the emissions with respect to photospheric magnetograms.

3.1. Time Profiles

The left-hand panels in Figure 1 show time profiles of the flare in hard X-rays at 25–250 keV observed by WBS, and the right-hand panels give the microwaves at 1–18 GHz observed by OVSA. For comparison, we also plot the *GOES* soft X-ray light curve at 1–8 Å (*dotted line*), the soft X-ray light curve from the SXT beryllium filter (*dot-dashed line*), and the low-energy hard X-rays from the HXT L channel (14–23 keV;

dashed line). Note that for this strong X5.6 event, the data counts in the HXT L channel exhibit overflow effects during much of the impulsive phase (19:16–19:23 UT).

Figure 1 shows that the flare emissions comprise two episodes. From 19:10 to 19:24 UT, hard X-ray and microwave emissions consist of a dozen impulsive bursts, each lasting for tens of seconds and being characterized by a sharp rise and a fast decay. Such temporal structures can be seen at both wavelengths through all energies and frequencies, suggesting a common mechanism to produce the electrons that emit the hard X-rays and microwaves. During the decay of soft X-rays, a gradual burst arises at around 19:28 UT in the hard X-ray and radio bands. At almost all hard X-ray energies and microwave frequencies, this emission is a single, gradual component lasting for about 10 minutes. For clarity throughout the following text, we term the episode from 19:10 to 19:24 UT the “impulsive phase” and emissions during this phase as the “impulsive component” or “impulsive burst.” Correspondingly, the episode from 19:28 onward is called the “gradual phase,” when the “gradual component,” or “gradual burst,” is present in the hard X-ray and microwave light curves.

In contrast to the impulsive bursts, the gradual-phase component shows some pronounced characteristics. First, the gradual component is a single burst, with a slowly varying time profile. The gradual microwave component has especially

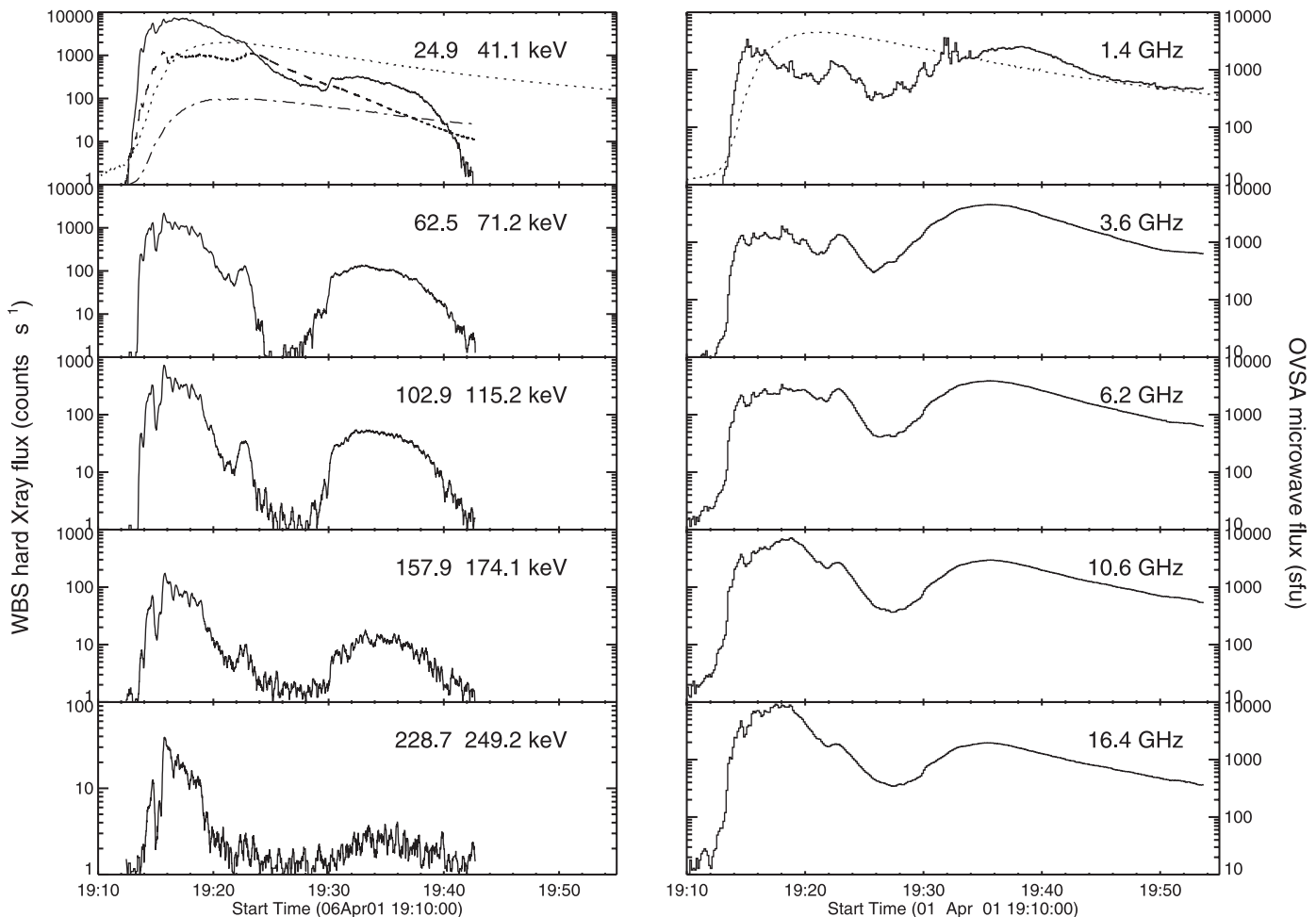


FIG. 1.—*Left*: Hard X-ray light curves from the WBS/HXS multiple-channel detector. *Right*: Microwave light curves from OVSA. In the top panels, the dotted line indicates the soft X-ray emission at 1–8 Å from *GOES*, the dashed line shows the HXT L-channel (13–23 keV) emission, and the dot-dashed line shows the soft X-ray emission observed by the SXT Be filter.

smooth and structureless light curves, and the rise and decay are almost symmetric. Second, the gradual hard X-ray component is most evident at energies above 20 keV. The top left-hand panel in Figure 1 shows that there is barely a counterpart in soft X-rays and the HXT L channel at the time when the gradual hard X-rays arise. Instead, soft X-rays exhibit a rather smooth decay during the gradual burst as a continuation from the late impulsive phase.

These observations suggest that at the rise of the gradual burst, a new injection of nonthermal electrons occurred. The lack of a prominent low-energy (<20 keV) counterpart, in contrast to the rise in the high-energy channels, possibly indicates that the spectral properties of the gradual component are different from those of the impulsive component, and such differences would reflect different physical mechanisms governing the plasma heating and particle acceleration during the flare. This point is further explored in detailed spectral analyses in the following sections.

3.2. Morphologies and Magnetic Properties

Soft X-ray, hard X-ray, and microwave images are obtained to study the spatial evolution of the flare at various wavelengths. In Figure 2, we show the time sequence of the hard X-ray contours derived from the HXT M1 (*top two panels*) and H (*bottom two panels*) channels, superposed on the soft X-ray images acquired from SXT with the beryllium filter, which is usually believed to represent emission by the hottest plasmas

in the coronal loops observed by SXT. In Figure 3, we also co-align the hard X-ray images at the HXT M1 and M2 channels (*white contours*) and microwave maps at a few frequencies (*black contours*) with the longitudinal magnetograms obtained from MDI on *SOHO*. In the two leftmost panels, we show the high-energy observations and the longitudinal magnetogram during the impulsive phase (at 19:16 UT). In the other three panels, we show hard X-rays and microwaves for the gradual component, and the background magnetograms are taken at the flare maximum (19:16 UT), preflare (19:00 UT), and postflare (20:57 UT) phases, from left to right. Note that hard X-ray images in the L channel are not presented in this paper because of an overflow problem that occurred in this channel during most of the impulsive phase.

Figures 2 and 3 show looplike structures in soft X-ray images and the locations of hard X-ray and microwave sources. Evolution of the hard X-ray and microwave source structures from the impulsive to the gradual phase suggests that the gradual component of the flare involves a new source that is different from that in the impulsive phase. For the impulsive component, the hard X-ray emission sources are rather complicated, with rapid evolution. In general, emissions at higher energies (M2–H) primarily emerge from two sources, denoted “A” and “B” in Figures 2 and 3, which are located at two ends of the soft X-ray loop structure and in strong magnetic fields of opposite polarities. Remarkably, Figure 3 shows that the magnetograms obtained by MDI

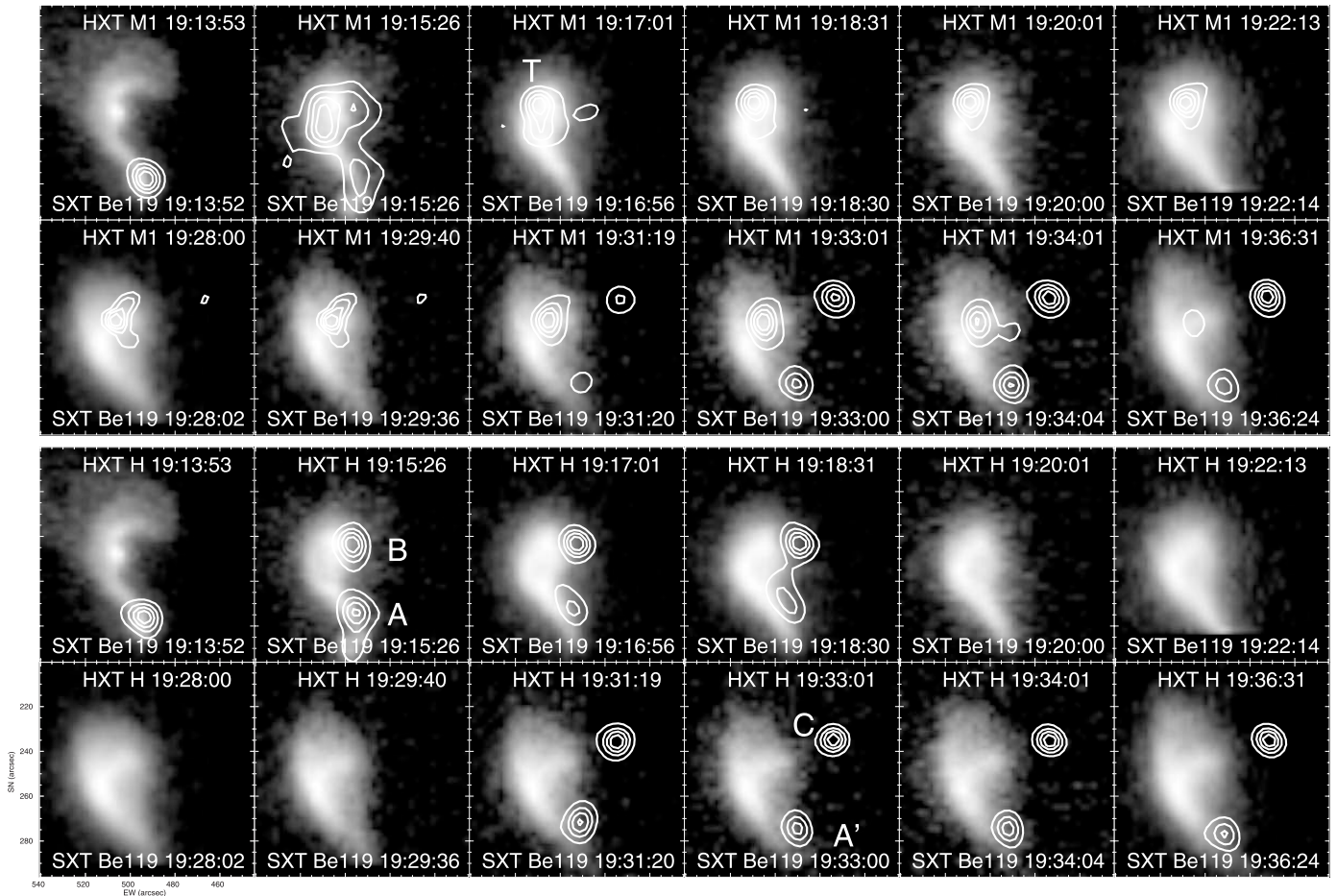


Fig. 2.—Evolution of the flare during the impulsive and gradual phases, as observed in soft X-rays (*images*) by the SXT Be filter and hard X-rays (*contours*) by the HXT M1 and H channels.

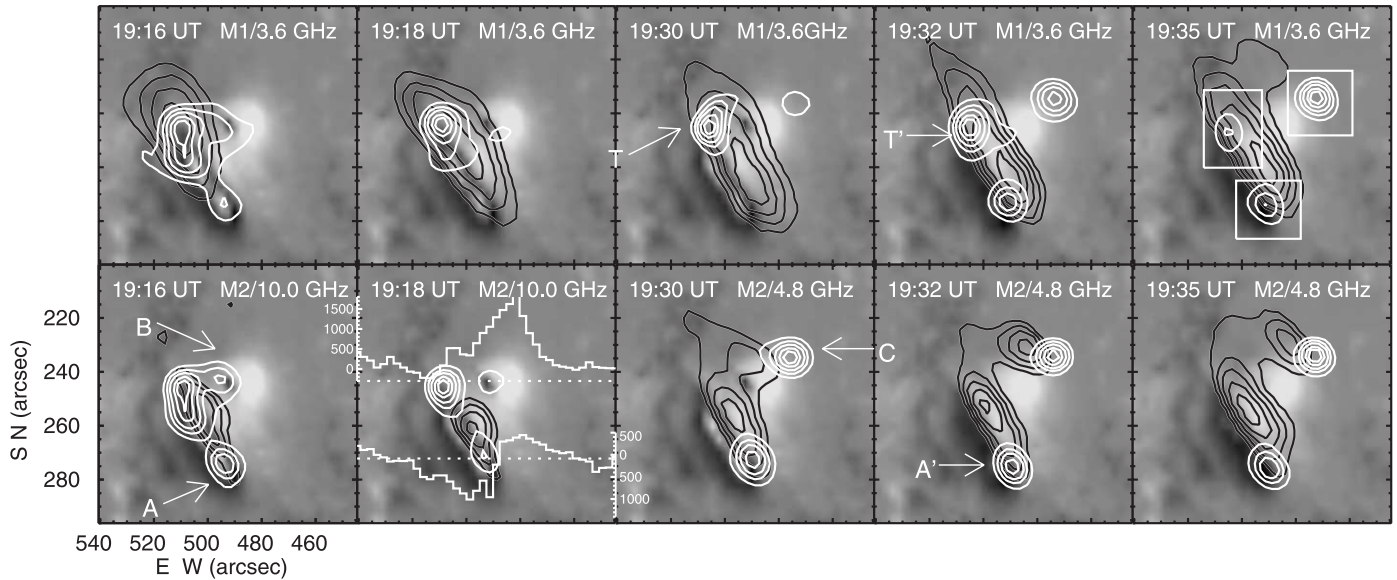


FIG. 3.—Evolution of the flare during the impulsive and gradual phases, as observed at hard X-ray and microwave wavelengths. White contours depict hard X-ray counts, the contour levels being 0.2, 0.35, 0.5, 0.7, and 0.85 of the maximum counts of each image. Black contours illustrate microwave brightness temperature, and the contour levels are 0.4, 0.55, 0.7, and 0.85 of the maximum for the impulsive component and 0.5, 0.6, 0.7, 0.8, and 0.9 of the maximum for the gradual component. The labels A, A', B, and C denote locations of the hard X-ray emissions at the footpoints, and the labels T and T' denote the hard X-ray loop-top sources. The white boxes around sources A', C, and T' indicate the areas of integration for the spatially resolved spectral analysis (see § 4.1). The gray-scale images show the MDI magnetograms. The magnetogram in the leftmost three columns is taken at 19:16 UT, showing the sites of a magnetic anomaly with a sign reversal observed during the impulsive phase (Qiu & Gary 2003). The magnetogram in the fourth column is obtained at 18:00 UT, and that in the rightmost panels is obtained at 20:57 UT. In the bottom panel of the second column, we also illustrate the profiles of the preflare (18:00 UT) magnetic flux density across sources A and B, the positions being indicated by white dashed lines. Images at all wavelengths are co-aligned, with solar rotation removed.

during the impulsive phase reveal strong magnetic anomalies at A and B, coinciding with the locations of the higher energy hard X-ray emission. The magnetic anomalies are measurement artifacts due to the temporary distortion of the profile of the magnetically sensitive lines. This is caused by the strong nonthermal beam impact on the lower atmosphere, where the magnetic fields are measured (Qiu & Gary 2003). The two sources A and B, therefore, represent conjugate footpoints of the flare loop structure, where electrons precipitate to the chromosphere to produce thick-target hard X-ray emission. At lower energies (<30 keV), most of the time during the impulsive phase, the hard X-ray emission resides in the coronal loop connecting A and B. The source denoted “T” in Figure 2 can be regarded as a loop-top source that is not visible in the HXT H channel, or ≥ 50 keV. The complexity of the hard X-ray morphology also suggests that the flare involves multiple loops.

Seen in Figure 3, in the impulsive phase, the microwave emission appears as an extended source connecting hard X-ray sources A and T, which represents emission from flare loops by trapped electrons. Figure 3 also shows that microwave emissions at all frequencies are dominantly from the location close to the negative magnetic fields. To understand the apparent asymmetry in the spatial distribution of microwave emission, we plot magnetic flux density profiles across sources A and B in the lower panels of the second column. Source A is located in the umbral area, where there are strong saturation effects in the measurements of magnetic fields (Liu & Norton 2001;¹ Qiu & Gary 2003). Taking into consideration the saturation effects, the magnetic fields at source A should be well above 1000 G, compared with less than 1000 G at source B.

Therefore, the spatial distribution of microwave emission in this event seems consistent with Wang et al. (1995), who found that microwaves are emitted by a source close to the footpoint with stronger magnetic fields.

During the gradual phase, starting from 19:28 UT, hard X-ray emission at the M2 and H channels exhibits a much simpler configuration, with two emission sources, A' and C, in opposite magnetic polarities. A' is located in negative magnetic fields very close to the impulsive source A, the displacement being of the order of $3''$ – $4''$, and source C lies in positive magnetic fields about $20''$ away from the previous emission source B. At lower energies, M1 and L, we find source T' located between A' and C and about $3''$ west of the impulsive source T. Microwave maps in Figure 3 show an extended source connecting A' and T' at various frequencies. The maps at 4.8 GHz also reveal another source near C in the positive magnetic field region. The hard X-ray and microwave emissions outline the configuration of a flare loop for the gradual component, in that higher energy (>30 keV) hard X-rays in the magnetic fields of opposite polarities represent conjugate footpoints A' and C, while the microwaves and lower energy hard X-rays show emission sources in or at the top of the loop connecting the two footpoints. That the gradual hard X-ray component at greater than 30 keV emerges from thick-target footpoint sources makes this event different from the events in which the gradual hard X-ray bursts are regarded to be from thin-target coronal sources emitted by trapped electrons (Kosugi et al. 1988; Tsuneta et al. 1984; Nitta et al. 1989).

In Figure 2 we also note a peculiarity that the gradual hard X-ray source C does not overlap with any part of the soft X-ray loop, which may shed some uncertainty on the configuration of the gradual component. This is perhaps because the soft X-ray loops seen by SXT largely show the hot remnant of the

¹ Liu & Norton (2001) is available at <http://soi.stanford.edu/general/TechNotes/01.144/TN01-144.pdf>.

impulsive component. The relation between the microwave sources and the magnetic fields suggests that A' and C are footpoints of a new coronal loop. In the following sections, we analyze the evolution of the hard X-ray sources and spatially resolved hard X-ray spectrum, which yields further evidence that A' and C are conjugate footpoints.

3.3. Spatial Evolution of High-Energy Sources

Hard X-ray observations also reveal the spatial evolution of the emission sources during both the impulsive and gradual phases. This is most evident by the apparent motion of the footpoints A, A', B, and C. Figure 4 (*left*) shows the evolution of the centroids of these footpoints, with respect to the magnetic neutral line, derived from HXT H-channel images. The centroid coordinates are defined as $X_0 = \Sigma(X_i C_i) / \Sigma C_i$ and $Y_0 = \Sigma(Y_i C_i) / \Sigma C_i$, where X_i , Y_i , and C_i are the X - and Y -coordinates and data counts in the i th pixel, and the integration is over the pixels with the data counts larger than 30% of the maximum. With these locations, we can determine the distance between the conjugate footpoints. In Figure 4 (*right*), we plot the evolution of the distance between A and B during the impulsive phase and between A' and C during the gradual phase.

For the impulsive component, the hard X-ray emission at B moves westward into stronger magnetic fields, while source A evolves northward (Fig. 4, *left*). From 19:14 to 19:18 UT, such motions bring the two footpoints closer with an average speed of 28 km s^{-1} (Fig. 4, *right*). That emission source B is evolving can be confirmed by the MDI magnetograms, which reveal a corresponding evolution of the magnetic anomaly produced by heating of the lower atmosphere (Qiu & Gary 2003), at the same place. During the gradual phase, source C evolves northwestward and source A' moves southward (Fig. 4, *left*), representing a systematic separation motion

between the two and away from the magnetic inversion line. From 19:30 to 19:40 UT, the average speed of the separation is 13 km s^{-1} (Fig. 4, *right*).

From the OVSA observations, we find that the microwave source in the positive magnetic fields also exhibits a westward motion during the gradual phase, as shown in Figure 3. The microwave source motion shown in the maps is verified by visibility measurements. The radio visibilities at multiple frequencies can be used to derive the measure of the separation of the double sources in real space, which reveals a gradual increase of the separation consistent with hard X-ray observations during the gradual phase.

Between 19:20 and 19:30 UT, because of insufficient data counts, poor hard X-ray images in the H channel give unreliable centroid locations. We have examined the time sequence of HXT M2-channel images during this period with a 20 s cadence. The footpoint sources A' and C first appear at 19:28 UT, and from the images, there is no sign of B and C being associated in any way, such as C being a result of continuous motion of B. Therefore, the gradual emission is rather an independent component from the impulsive burst.

It is usually regarded that the observed motion of flare emission at the footpoints reflects continuous magnetic reconnection, the most pronounced examples of which are the well-known two-ribbon flares produced by progressive magnetic reconnection at rising altitudes in the corona (see review by Švestka & Cliver 1992). The observed hard X-ray source motion can be understood in the same context; i.e., magnetic reconnection proceeds continuously, and electrons precipitate into neighboring regions successively (e.g., Sakao 1999; Masuda, Kosugi, & Hudson 2001). The multiple peaks during the impulsive phase may well be produced by such successive energy release in complicated structures. During the gradual phase, in contrast, the separation motion of A'

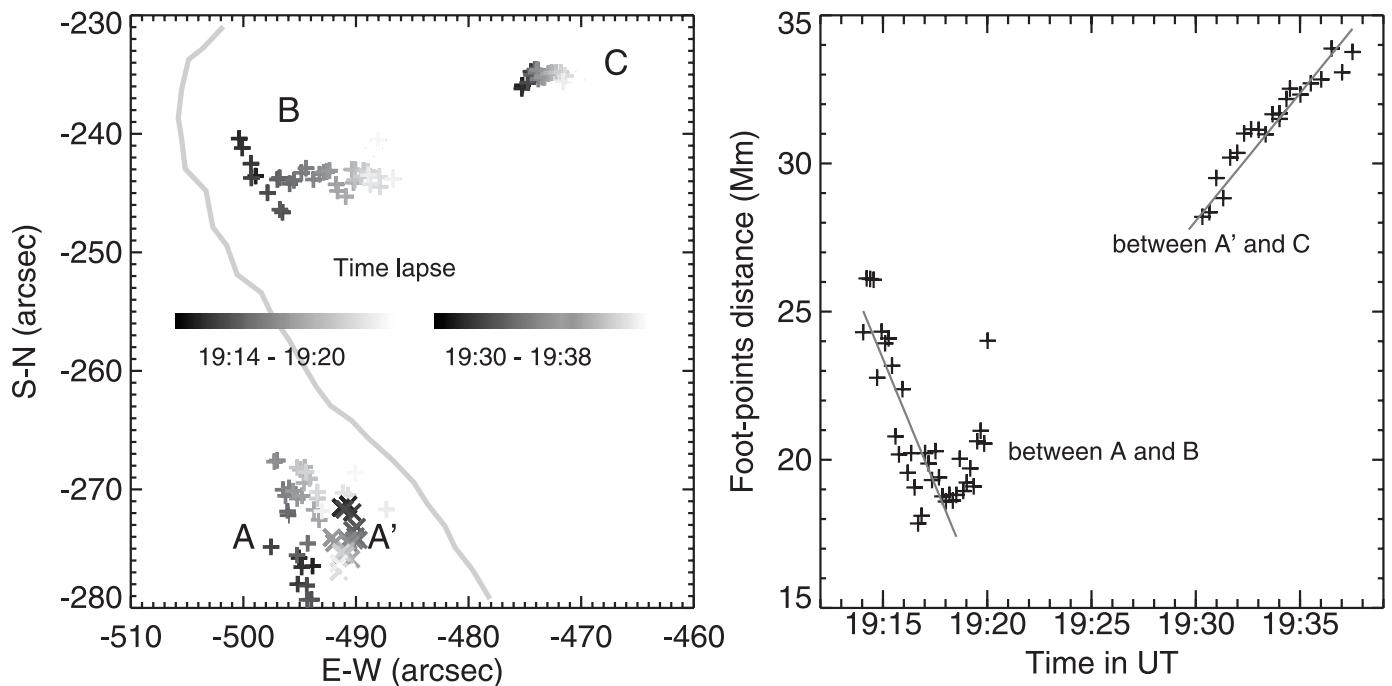


FIG. 4.—*Left*: Evolution of the centroids of the hard X-ray sources observed by HXT in the H channel for the impulsive and gradual components. The gray curve outlines the longitudinal magnetic neutral line derived from the magnetogram at 18:00 UT. *Right*: Evolution of the distance between sources A and B during the impulsive phase and between A' and C during the gradual phase. The straight lines indicate the linear least-squares fits of the distances.

and C at greater than 50 keV is more organized and almost perpendicular to the magnetic neutral line (Fig. 4, *left*). Such systematic separation indicates magnetic reconnection in a manner similar to two-ribbon flares, which further confirms that A' and C are very likely conjugate footpoints of a bipolar arcade formed by progressive magnetic reconnection at rising altitudes. That the pattern of the footpoint motion in the gradual phase is different from that in the impulsive phase also supports the idea that the impulsive and gradual components involve different magnetic structures in which the energy release takes place.

4. SPECTRAL EVOLUTION

We analyze the hard X-ray photon spectrum and microwave total power spectrum to infer the spectra of electrons emitting at the two wavelengths for both the impulsive and gradual bursts. By assuming that the hard X-ray and microwave electrons have a power-law distribution, $n(E) = AE^{-\delta}$, we can derive the power-law index δ and the total number of nonthermal electrons emitting hard X-rays and microwaves. These parameters and their evolution reflect the properties of acceleration and trapping that produce emissions at the two wavelengths.

The hard X-ray spectral analysis is conducted with only HXT data using the HXT calibration information (Sato et al. 1998). WBS data are not analyzed, for lack of a reliable spectral calibration. For the gradual component, the spectral parameters are obtained for spatially resolved hard X-ray sources as well. Since the gradual component has a much lower count rate, we use the *pixon* algorithm (Metcalf et al. 1996) to obtain hard X-ray images with 1 minute integration in order to achieve optimal photometry. We convert the ratio of data counts from different HXT energy channels into the photon spectral index γ_X . Then we derive the electron power index $\delta_X = \gamma_X + 1.5$ for thick-target sources. When suitable, we also fit the loop-top source to a thermal spectrum, to derive temperature and emission measure (EM) of the loop-top plasmas that possibly contribute to low-energy (<30 keV) hard X-rays.

Several problems in the hard X-ray spectral analysis should be acknowledged. First, because of both the overflow problem and a very likely mixture of thermal and nonthermal contributions to the HXT L-channel emission, the data in the L channel during the impulsive phase are not used in the spectral analysis. Second, for such a strong (X5.6) event, pulse pileup (Kane & Hudson 1970) in different energy channels will distort the spectral analysis. Therefore, the spectral parameters derived during most of the impulsive phase (between 19:16 and 19:25 UT) may not be reliable. Furthermore, we realize that the results from the hard X-ray spectral analysis are obtained from fewer than four energy channels, which unavoidably limits the accuracy of fits to a power-law spectrum. Nevertheless, the results presented below can still serve to illustrate quasi-quantitatively the different spectral properties and evolutionary trends between the impulsive and gradual components.

For microwaves, we fit the total power spectrum, as shown in Figures 5a–5e, to obtain the slope α of the optically thin part. During the impulsive phase of the burst, the microwave spectrum is still rising at 18 GHz, so no optically thin part of the spectrum can be measured. For the gradual component, we fit the optically thin part of the microwave spectrum to a power law and then use the formulae by Dulk & Marsh

(1982) to convert the index α to the electron index $\delta_r = (1.22 - \alpha)/0.90$.

4.1. Hard X-Ray and Microwave Spectral Evolution

Figure 5f shows the electron index $\delta_X = \gamma_X + 1.5$ derived from the ratio of the total counts from the M2 and H channels. The δ_X derived in this way is an approximation of the spectral index of the precipitating electrons, since emissions in the M2 and H channels are dominated by footpoint sources during both the impulsive and gradual phases. In the early impulsive phase up to 19:16 UT, when the pulse pileup and thermal contribution are likely ignorable, δ_X varies between 5 and 7 and exhibits an SHS trend over individual peaks. For the gradual component, δ_X continuously decreases, from 4.5 at 19:30 UT to 3.5 at 19:40 UT, reflecting an SHH evolution pattern. On average, the precipitating electrons have a harder spectrum during the gradual phase than during the impulsive phase. These spectral characteristics of the impulsive and gradual bursts are consistent with previous results (Silva et al. 2000).

We fit the optically thin part ($f \geq 10$ GHz) of the microwave total power spectrum during the gradual phase to get the slope of the flux density versus frequency and use approximation formulae by Dulk & Marsh (1982) to obtain the power-law index δ_r . Figure 5f shows that δ_r varies from 2 to 2.5 from 19:30 to 19:35 UT and then slightly flattens after the maximum. The electron spectrum from microwaves is also harder than the spectrum of electrons emitting hard X-rays, with $\delta_X - \delta_r \approx 1.5$. Keep in mind that the spectral analysis of HXT data covers only a limited energy range of 23–93 keV. That hard X-rays and microwaves do not yield the same power-law index may indicate that the higher energy electrons, which emit the microwaves, have a harder spectrum.

Figure 5g shows the number of nonthermal electrons emitting hard X-rays and microwaves. Although we cannot calculate the total number of microwave-emitting electrons during the impulsive phase, a direct comparison of the microwave-to-hard X-ray flux ratio between the impulsive and gradual components shows that the gradual component is a microwave-rich event, which is an indication of stronger trapping during the gradual phase.

With the parameters derived from the hard X-ray imaging and spectral analysis, we can also estimate the total energy flux deposited at the footpoints by nonthermal electrons during the impulsive and gradual phases. We find that if we integrate electron energy from over 30 keV, the energy flux during the gradual phase is smaller than that during the impulsive phase by a factor of 20. This factor becomes even bigger if we integrate from a lower energy, such as 10 keV. Because of the much smaller energy flux deposited at the chromosphere by electrons during the gradual phase, the chromospheric evaporation should also be much weaker than during the impulsive phase. This probably explains the apparent deficiency of the gradual soft X-ray component.

4.2. Spatially Resolved Hard X-Ray Spectrum

Hard X-ray observations obtained by HXT can provide information on spatially resolved spectral evolution. To help understand the nature of the gradual component, we analyze the X-ray spectra at the sources A', C, and T'. For better photometry, we apply the *pixon* algorithm (Metcalf et al. 1996) to construct hard X-ray images with a 1 minute cadence during the gradual phase and integrate the total counts at each

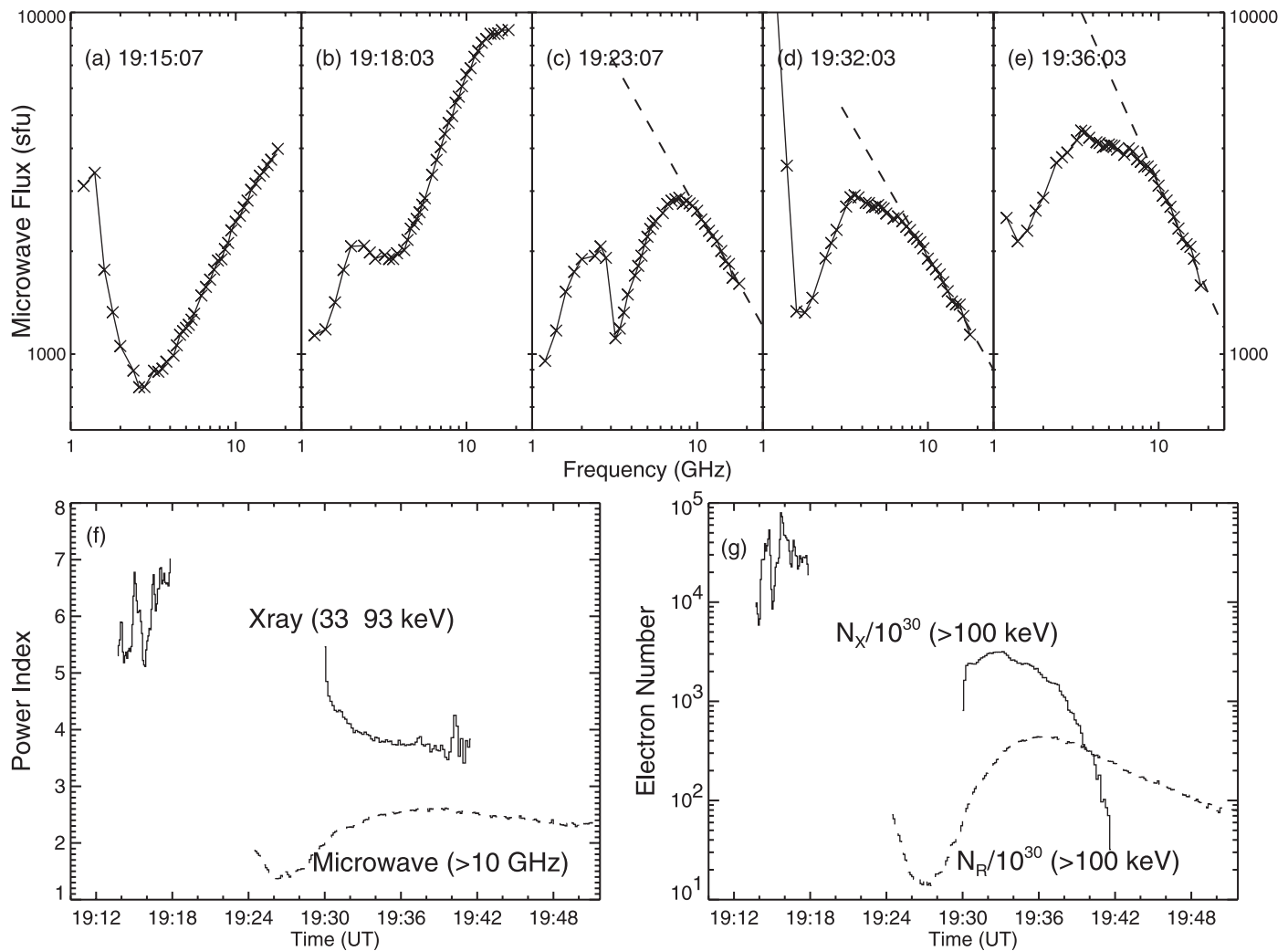


FIG. 5.—(a–e) Microwave total power spectrum during the impulsive and gradual phases. The dashed lines in the rightmost three panels show the least-squares fit of the optically thin part of the spectrum. (f) Electron power-law indices obtained from hard X-rays (solid line) and microwaves (dashed line). For hard X-rays, the index is obtained from the two-channel (M2–H) ratio. For microwaves, the index of the impulsive component is not given, for lack of a measurable optically thin part of the spectrum. (g) Total number of electrons emitting thick-target hard X-rays (solid line) and microwaves (dashed line).

source for the spectral analysis. The regions of integration are indicated in Figure 3 by white boxes around the three sources, which have a size of around 25'' by 25'' each.

Figure 6 (left) shows the power-law indices of the electron spectra at A' and C derived by fitting the M1-, M2-, and H-channel emissions with a power-law distribution. In this paper, we do not use the L-channel emission at A' and C, because most of the emission in L is observed at the loop top, and the photometry at the footpoints is very poor. Given the uncertainties in the analyses, the obtained power-law indices at A' and C can be regarded as identical, and their evolution is well correlated. This suggests that 20–90 keV hard X-rays at the two sources A' and C are emitted by the same population of accelerated electrons. This provides further evidence that A' and C are conjugate footpoints into which nonthermal electrons precipitate simultaneously to produce thick-target emissions.

The loop-top source T' is observed only at L and M1 channels. In the M2 and H channels, the loop-top emission is barely detected, the integrated photon counts being less than 1% of the footpoint source counts. The ratio of photon counts in the M1 channel to those in the L channel is too small to

yield a reasonable value of the power-law index if we presume a power-law distribution of electrons. If we assume that the loop-top source below 30 keV is thermal emission by isothermal coronal plasmas during the gradual phase, we can try to investigate the properties of this source. First, we use the temperature (T_e) and EM derived from GOES two-channel soft X-ray observations to evaluate the thermal contribution of the plasmas emitting at GOES wavelengths to the L- and M1-channel emission (Fig. 6, middle and right). Figure 7 shows the evolution of T_e and EM, which both decay smoothly from the impulsive to the gradual phase, and Figure 6 (middle and right) shows that the contribution of these thermal plasmas accounts for only about 10% of the observed counts in the M1 channel and less than 50% in the L channel. Therefore, the loop-top emission observed in the L and M1 channels is not entirely from thermal plasmas emitting at GOES wavelengths. Alternatively, using the HXT calibration table, we can also convert the counts ratio at the L and M1 channels to T_e and EM. This analysis yields a higher temperature (27 MK) and lower EM during the gradual phase, as also plotted on Figure 7. Taking into account the size of the loop-top source, the HXT parameters give a loop-top density of the order of

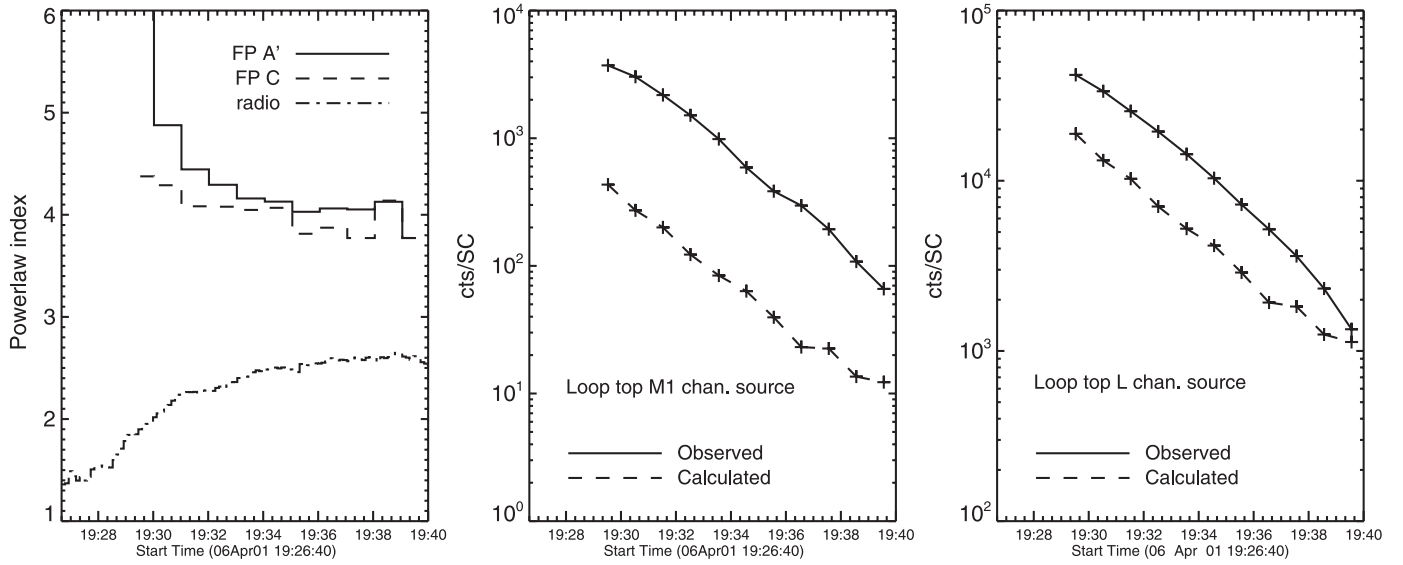


FIG. 6.—*Left*: Electron power-law indices at sources A' and C derived from the spatially resolved hard X-ray images at the HXT M1, M2, and H channels for the gradual component. The dot-dashed line shows the power-law index of microwave-emitting electrons. *Middle*: Observed and calculated data counts from the loop-top source during the gradual phase at the HXT M1 channel. *Right*: Observed and calculated data counts from the loop-top source during the gradual phase at the HXT L channel. The solid lines in the middle and right-hand panels indicate the total counts integrated from the images of the loop-top source T'. The dashed lines indicate the calculation of the thermal bremsstrahlung emission, with the parameters of temperature and EM derived from analyzing *GOES* data under an isothermal assumption.

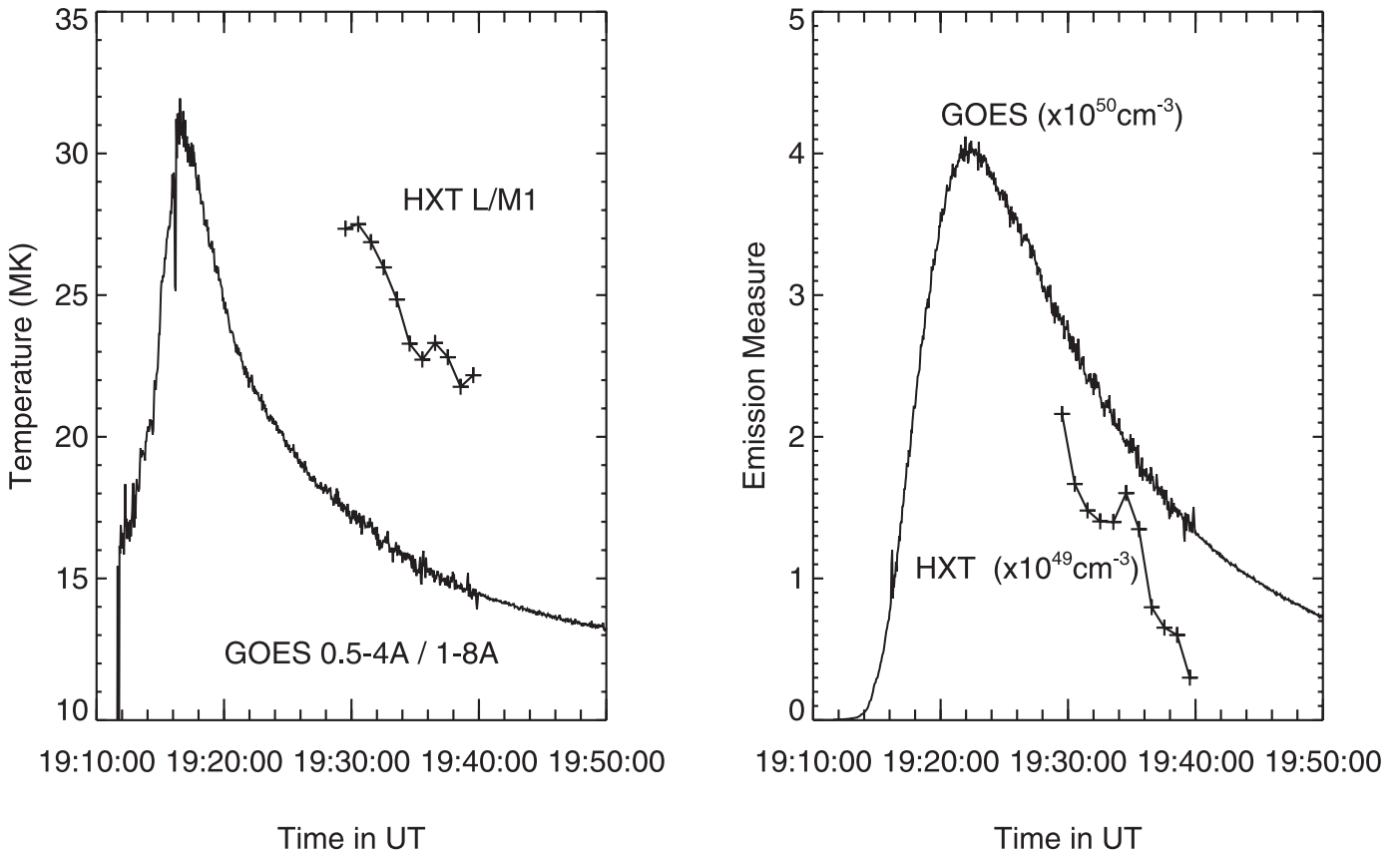


FIG. 7.—Evolution of the temperature (*left*) and emission measure (*right*) derived from *GOES* soft X-ray observations throughout the flare and from spatially resolved HXT L- and M1-channel observations of the loop-top source during the gradual phase.

10^{11} cm^{-3} during the gradual phase. These values are reasonable parameters for flare loops and suggest that the loop-top X-rays might be dominantly thermal emission by hot plasmas. It is probable that any hot loop-top component generated during the gradual phase is, however, masked by the nearby decaying impulsive component that may also comprise high-temperature (27 MK) plasmas, as judged from the smooth and monotonic decay from the impulsive to the gradual phase observed by *GOES*, *SXT*, and *HXT* at the L channel. There may also exist a loop-top nonthermal source that primarily emits hard X-rays below 30 keV during the gradual phase, but such a source would be too weak to distinguish from the decaying impulsive component.

The spectral morphology of the gradual hard X-rays in this event thus appears similar to that of most impulsive flares with loop-top emission at low energies, most likely by thermal plasmas, and higher energy hard X-rays from conjugate footpoints by precipitating electrons. In the past, a few hard X-ray imaging observations by *Hinotori* revealed that gradual hard X-ray components are emitted by either very hot plasmas or trapped electrons (Tsuneta et al. 1984; Nitta et al. 1989) at the top of the coronal loop. Given the coarse spatial resolution ($15'' \sim 30''$) and the relatively low energy range ($\leq 50 \text{ keV}$) of the imaging instruments before *Yohkoh*, it is likely that in the gradual events reported earlier the footpoint thick-target sources were not resolved from the dominating loop-top source. Furthermore, the *Hinotori* hard X-ray imagers were likely to be sensitive to energies lower than its nominal energy ranges, which made it difficult to isolate a loop-top nonthermal source from thermal emission. The observations of the present event provide, for the first time, clear evidence of thick-target footpoint emission of hard X-rays during a gradual burst.

The dominance of these thick-target sources shows that the gradually hardening hard X-ray spectrum cannot be explained by nearly perfect trapping of nonthermal electrons at the loop top. We must consider other scenarios to explain the hardening of the gradual-phase spectrum. It is probable that the acceleration mechanism during the gradual phase is fundamentally different from that during the impulsive phase. We also note that the hard X-ray and microwave time profiles exhibit energy-dependent time lags during the gradual phase. In the next section, we conduct time lag analysis to articulate the extent of time lags shown in both wavelengths, which will provide more information on precipitation and trapping of electrons produced by the gradual-phase mechanism.

5. TIME LAG ANALYSES

In this section, we conduct a time lag analysis on the hard X-ray light curves, to derive the energy-dependent time lags for both the impulsive and gradual bursts. We also briefly examine the time lags between hard X-rays and microwaves for the two bursts. The derived parameters may be used to infer the existence of different acceleration mechanisms for the impulsive and gradual bursts.

To derive time lags in hard X-rays, we exclusively use WBS HXS pulse-height data obtained in 32 energy channels. For the impulsive component, data counts are significant with respect to the background noise level at over 300 keV, and for the gradual burst, counts are significant at over 200 keV. The hard X-rays at around 40–50 keV are taken as a reference in order to avoid both thermal contamination at lower energies and the greater noise level toward higher energies. To obtain the time lags, a correlation analysis is the most straightforward method on light curves with multiple peaks,

as in the impulsive phase. For the gradual bursts, we also measure the peaking times of the hard X-ray bursts at changing energies with respect to the 40–50 keV burst.

For the impulsive component, we apply the correlation analysis to hard X-ray light curves from 19:14 to 19:19 UT, finding that hard X-rays at $\sim 300 \text{ keV}$ lag the emission at 40 keV by about 2 s. However, since it takes 2 s for the WBS HXS instrument to go through all 32 channels, the measured delay of 2 s might not be significant. We therefore regard there to be no significant energy-dependent time lag that is detectable by the observing instruments for the impulsive phase.

The gradual hard X-ray emissions exhibit certain short-timescale variations. It is of interest to understand whether these are significant features and how they compare in different energy channels. We apply a correlation analysis to the hard X-ray light curves, with the slow trend ($>60 \text{ s}$) removed, and find that these rapidly varying signals at different energies are not correlated with each other, the cross-correlation coefficient being smaller than 20%. Furthermore, for the gradual component, the microwave emission at almost all frequencies exhibits a very smooth profile with no fine structures. These facts indicate that the fine structures visible in hard X-rays are most likely statistical noise. This is different from the impulsive burst, which consists of a large number of spikes at timescales of a few seconds.

We apply a correlation analysis to the gradual bursts, which yields energy-dependent time lags $\tau_1(\epsilon)$, as plotted in Figure 8. The figure shows that for the gradual component, hard X-rays at higher energies lag emissions at lower energies systematically, the 200 keV X-rays being delayed by 20 s with respect to hard X-rays at 40–50 keV. These time lags are much larger

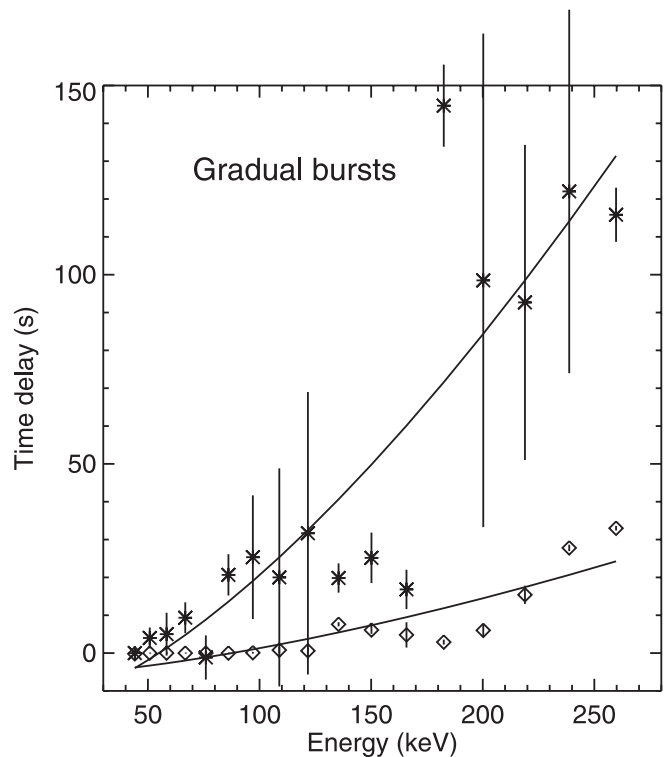


FIG. 8.—Average time lags of the gradual hard X-ray emissions at different energies relative to 41–47 keV emission, derived from the peaking times (asterisks) and the correlation analysis (diamonds). Solid lines indicate least-squares fits of the displayed data. Vertical bars indicate the standard deviations.

than those during the impulsive phase. Figure 1 also shows that during the gradual phase, hard X-rays at different energies do not peak simultaneously, with hard X-rays at lower energies reaching the maximum earlier than hard X-rays at higher energies. Therefore, we derive and compare the peaking times of hard X-rays at different energies. To avoid spurious signals, we apply to the data a low-pass filter with a changing cutoff value from 20 to 120 s. In Figure 8, we plot the mean of the peaking times $\tau_2(\epsilon)$ over different cutoff values with respect to the maximum time at 40 keV. The figure shows that the hard X-ray emission peak at 200 keV is delayed by almost 100 s compared with hard X-rays at 40–50 keV.

To examine time lags between emissions at hard X-rays and microwaves, we apply correlation analysis to hard X-rays and microwaves that are interpolated to the same time grids. The analysis is performed for the impulsive and gradual bursts separately. Since there is no apparent time lag between microwaves at different frequencies, we only present the time delays between microwaves at 18 GHz and hard X-rays at changing energies from 30 to 300 keV. We find that during the impulsive phase, there is no difference in the peak times within the time resolution of the instruments (4 s). For the gradual burst, however, Figure 9 shows that the gradual microwaves lag the hard X-rays at all energies and that the amount of time delay is very large at low energies. With respect to the 40–50 keV hard X-rays, the microwaves lag by about 100 s.

These observations add more information on the precipitation and trapping of electrons that are produced by the physical mechanism during the gradual phase. Coordinated observations show several lines of evidence that the gradual burst in this event is produced by a mechanism that is different from that in the impulsive phase. First, spatial evolution indicates magnetic reconnection during the gradual phase in an organized pattern different from that in the impulsive component. Second, the hard and hardening spectrum is likely produced by a mechanism that keeps generating ever higher energy electrons in the gradual phase. Third, the significant time lags and a greater microwave-to-hard X-ray flux ratio for the gradual bursts suggest stronger trapping of higher energy electrons during the gradual phase, which again points to a different mechanism for the gradual burst, compared with the impulsive bursts. These observations suggest clues to a candidate acceleration mechanism to explain the observed properties, which is discussed in the next section.

6. ACCELERATION IN “COLLAPSING” MAGNETIC TRAPS

In the foregoing sections, we provide comprehensive analyses of an X5.6 flare from the impulsive to the gradual

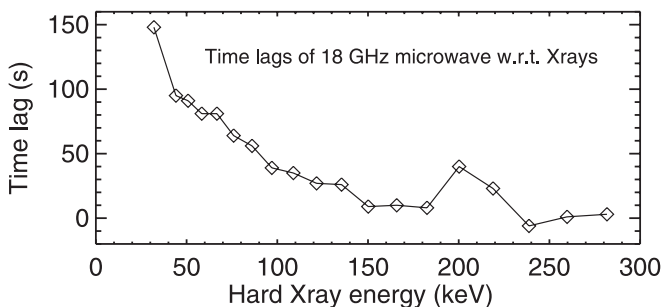


FIG. 9.—Time lags of 18 GHz microwaves with respect to hard X-rays at 30–300 keV for the gradual burst.

phase. Our results show contrasting temporal and spectral properties between the impulsive and gradual bursts, consistent with the statistical results obtained by Kosugi et al. (1988) and Silva et al. (2000). The new information from this study is that hard X-rays at ≥ 30 keV are thick-target sources emitted by precipitating electrons at conjugate footpoints of flare loop(s) during both the impulsive and gradual phases. This is the most important result, and it opposes the scenario that the gradual hard X-ray component is a result of thin-target emission by electrons trapped in the corona (e.g., Kosugi et al. 1988). An alternative physical mechanism is hence required to explain the observed properties of the gradual burst in this event.

Based on the observations, we present the scenario of continuous acceleration by a stochastic mechanism. Such an acceleration mechanism picks up seed electrons that have already been accelerated—for example, by an electric field generated in magnetic reconnection—to relatively low energies and continues to accelerate them to higher energies over a fairly long timescale.

A candidate stochastic acceleration mechanism has been considered by Somov & Kosugi (1997) in a schematic model. They propose a two-step acceleration as a result of magnetic reconnection. In the first step, electrons are accelerated to tens of keV by a super-Dreicer electric field generated inside the reconnecting current sheet. The magnetic reconnection also generates fast outflows that may further produce fast shock waves between the reconnected field lines and the closed magnetic loops underneath. Meanwhile, the preaccelerated electrons are carried downward by the reconnected magnetic field lines that move out of the reconnection region, and then get reflected by the shock front. This is called a “collapsing” magnetic trap by Somov & Kosugi (1997). The preaccelerated electrons can be further accelerated between the collapsing trap and the upstream fast shock waves by the collapsing-trap effect, or a first-order Fermi-style acceleration, and by the fast shocks as well. The proposed mechanism can accelerate seed electrons to very large energies when the trapping timescale approaches the lifetime of the collapsing trap, which is of the order of several to tens of seconds, depending on the length and collapsing velocity of the trap.

Somov & Kosugi (1997) introduced second-step acceleration via the collapsing trap to interpret the temporal and spectral evolution and spatial distribution of gradual hard X-rays. Qualitatively, this mechanism may explain the gradual burst in this event. The continuous acceleration of electrons accounts for the hard and hardening spectrum during the gradual phase. That electrons can be efficiently accelerated by this mechanism requires trapping of these electrons for a sufficiently long time before leaking to precipitation, which further requires a low density of the trap. Such a requirement is advantageous in explaining the deficiency of nonthermal, thin-target emission in this event, in contrast to the event reported by Masuda et al. (1994), which has a loop-top, non-thermal source. The large, energy-dependent time lags can be viewed as a result of the continuous acceleration and trap-plus-precipitation by Coulomb collisions in a low-density trap. Efficient trapping and continuous acceleration also produce the large flux and time lags of microwaves that are likely emitted by electrons with even higher energies, namely, several hundred keV to MeV (Kosugi et al. 1988; Nitta & Kosugi 1986). Furthermore, it is probable that the density at the energy release site is also low, so that heating by the reconnection electric field is less efficient (Tsuneta 1985; Holman 1985).

The viability of the collapsing-trap model can be supported by the spatial evolution of the gradual component in this event. Observations show regular separation motion of the two footpoints, resembling a standard two-ribbon flare that is produced by continuous magnetic reconnection at progressively higher altitudes in a bipolar magnetic configuration. Previous limb observations of such standard flares often suggest the “shrinkage” of newly formed magnetic loops from the *Y*-type reconnection point (e.g., Forbes & Acton 1996). This picture is consistent with the configuration of the collapsing trap, and the progressive magnetic reconnection also continuously generates fast shock waves and the collapsing trap to sustain the continuous acceleration.

Certainly, for the collapsing-trap model to account for the gradual burst in this event, the model has to be formulated to yield a realistic pitch-angle distribution and energy deposit rate at the loop top and at the footpoints, in order to check quantitatively with the observations.

7. CONCLUSIONS

In this study, we are interested in finding the mechanism of nonthermal emissions for the gradual component. This can be studied in terms of spatial and spectral evolution at energies corresponding to the nonthermal emission. Through this analysis, we find that the gradual burst is produced by a physical mechanism different from that for the impulsive components, at least in this particular event. Below we present the major results from this study.

Most importantly, we can identify the source regions of the hard X-ray and microwave emissions from the spatially resolved observations. We find that for this event, both the impulsive and gradual hard X-rays at ≥ 30 keV are thick-target sources located at the footpoints of flare loops. We also find that the gradual hard X-rays and microwaves evolve smoothly in a separation motion of the two sources above 50 keV, and the spatially resolved spectral analysis shows that the two sources have identical spectral evolution within the limitations of the data. These are signs of progressive magnetic reconnection and subsequent electron precipitation at conjugate footpoints during the gradual phase. These results oppose the view that the gradual burst is thin-target emission produced by electrons entirely trapped in the corona but agree with the view of MacKinnon et al. (1986), who believed that hard X-rays in both components are thick-target sources, although in their study MacKinnon et al. (1986) lacked spatially resolved observations to verify their idea.

We derive contrasting properties of the impulsive and gradual bursts in terms of the temporal and spectral evolution.

The impulsive bursts consist of many short-timescale spikes, each exhibiting the SHS spectral evolution, while the gradual burst is a structureless single peak undergoing a gradual evolution over a timescale of about 10 minutes, with a continuously hardening spectrum. On average, the gradual burst also has a much harder spectrum than the impulsive burst. These are consistent with the results of Kosugi et al. (1988) and Silva et al. (2000). Observations also show that for the gradual burst, the higher energy hard X-rays systematically lag the lower energy hard X-rays, the amount of the time lag between the 40 and 200 keV hard X-rays being about 20 s. These large time lags cannot be explained by the energy-dependent energy-loss rate in a coronal trap, since the hard X-ray sources are primarily thick-target. The temporal and spectral properties of the gradual component requires a physical mechanism that continuously accelerates electrons to ever higher energies.

In terms of the relationship between hard X-rays and microwaves, we confirm the previous findings (Kosugi et al. 1988; Silva et al. 2000) that (1) the microwaves exhibit a large delay of several tens of seconds with respect to hard X-rays for the gradual burst, while there is no observable time delay, within the instrument accuracy, during the impulsive bursts; and (2) the gradual burst is microwave-rich in comparison with the impulsive bursts. These findings usually indicate that trapping of the electrons that produce microwave emissions is stronger for the gradual burst than for impulsive bursts.

On the basis of the observations, we propose that the gradual-phase electrons receive continuous acceleration by the collapsing-trap mechanism that was put forward by Somov & Kosugi (1997). The observed regular footpoint motion is the indication of progressive *Y*-type magnetic reconnection, which is in support of the configuration for the collapsing-trap mechanism. We also suggest that the trap density is low in this event, which favors trapping and continuous acceleration over a long timescale and as well explains the deficiency of loop-top emission, the large time lags, and the large flux ratio of microwaves to hard X-rays observed in this event.

The authors thank the *Yohkoh* and MDI teams for data service. We thank the referee for constructive comments and suggestions which help improve the manuscript significantly. This work is supported by the NASA grants NAG5-10212 and NAG5-10891. The OVSA is supported by the NSF grant AST 03-07670 to New Jersey Institute of Technology.

REFERENCES

- Aschwanden, M. J., Bynum, R. M., Kosugi, T., Hudson, H. S., & Schwartz, R. A. 1997, *ApJ*, 487, 936
- Bai, T., & Ramaty, R. 1979, *ApJ*, 227, 1072
- Domingo, V., Fleck, B., & Poland, A. I. 1995, *Sol. Phys.*, 162, 1
- Dulk, G. A., & Marsh, K. A. 1982, *ApJ*, 259, 350
- Forbes, T. G., & Acton, L. W. 1996, *ApJ*, 459, 330
- Gary, D. E., & Hurford, G. J. 1990, *ApJ*, 361, 290
- Högbom, J. A. 1974, *A&AS*, 15, 417
- Holman, G. D. 1985, *ApJ*, 293, 584
- Kane, S. R., & Hudson, H. S. 1970, *Sol. Phys.*, 14, 414
- Kosugi, T., Dennis, B. R., & Kai, K. 1988, *ApJ*, 324, 1118
- Kosugi, T., et al. 1991, *Sol. Phys.*, 136, 17
- Liu, Y., & Norton, A. A. 2001, MDI Measurement Errors: The Magnetic Perspective, SOI Tech. Note 01-144 (Stanford: Stanford-Lockheed Inst. Space Res.)
- Lu, E. T., & Petrosian, V. 1990, *ApJ*, 354, 735
- MacKinnon, A. L. 1988, *A&A*, 194, 279
- . 1991, *A&A*, 242, 256
- MacKinnon, A. L., Costa, J. E. R., Kaufmann, P., & Dennis, B. R. 1986, *Sol. Phys.*, 104, 191
- Masuda, S., Kosugi, T., Hara, H., Tsuneta, S., & Ogawara, Y. 1994, *Nature*, 371, 495
- Masuda, S., Kosugi, T., & Hudson, H. S. 2001, *Sol. Phys.*, 204, 55
- Melrose, D. B., & Brown, J. C. 1976, *MNRAS*, 176, 15
- Metcalf, T. R., & Alexander, D. 1999, *ApJ*, 522, 1108
- Metcalf, T. R., Hudson, H. S., Kosugi, T., Puetter, R. C., & Piña, R. K. 1996, *ApJ*, 466, 585
- Miller, J. A., LaRosa, T. N., & Moore, R. L. 1996, *ApJ*, 461, 445
- Nitta, N., Kiplinger, A. L., & Kai, K. 1989, *ApJ*, 337, 1003
- Nitta, N., & Kosugi, T. 1986, *Sol. Phys.*, 105, 73

- Qiu, J., & Gary, D. E. 2003, *ApJ*, 599, 615
- Sakao, T. 1994, Ph.D. thesis, Univ. Tokyo
- . 1999, *Proc. Nobeyama Symp., Solar Physics with Radio Observations*, ed. T. S. Bastian, N. Gopalswamy, & K. Shibasaki (NRO Rep. 479; Nagano: Nobeyama Radio Obs.), 321
- Sato, J., Kosugi, T., & Makishima, K. 1999, *PASJ*, 51, 127
- Sato, J., Sawa, M., Masuda, S., Sakao, T., Kosugi, T., & Sekiguchi, H. 1998, *The Yohkoh HXT Image Catalog* (Nagano: Nobeyama Radio Obs.)
- Scherrer, P. H., et al. 1995, *Sol. Phys.*, 162, 129
- Silva, A. V. R., Wang, H., & Gary, D. E. 2000, *ApJ*, 545, 1116
- Somov, B. V., & Kosugi, T. 1997, *ApJ*, 485, 859
- Švestka, Z., & Cliver, E. W. 1992, in *Eruptive Solar Flares*, ed. Z. Švestka, B. V. Jackson, & M. E. Machado (LNP 399; Berlin: Springer), 1
- Takakura, T., & Kai, K. 1966, *PASJ*, 18, 57
- Tsuneta, S. 1985, *ApJ*, 290, 353
- Tsuneta, S., et al. 1984, *ApJ*, 280, 887
- . 1991, *Sol. Phys.*, 136, 37
- Vilmer, N., Kane, S. R., & Trotter, G. 1982, *A&A*, 108, 306
- Wang, H., Gary, D. E., Zirin, H., Schwartz, R. A., Sakao, T., Kosugi, T., & Shibata, K. 1995, *ApJ*, 453, 505
- Yoshimori, M., et al. 1991, *Sol. Phys.*, 136, 69